

## Manufacture of Some Ferrite Compounds with Hexagonal Crystalline Structure and Study of their Structural Properties

Raed Aidan Najm<sup>1</sup> and Abdel Samie Fawzi Abdel Aziz<sup>2</sup>

<sup>1,2</sup>Department of Physics, College of Science, University of Tikrit, IRAQ.

<sup>1</sup>Corresponding Author: raedaidannajm@gmail.com



www.jrasb.com || Vol. 2 No. 4 (2023): August Issue

Received: 05-09-2023

Revised: 06-09-2023

Accepted: 08-09-2023

### ABSTRACT

PbFe<sub>12</sub>O<sub>19</sub> from this mixture and BaFe<sub>12</sub>O<sub>19</sub> And (Pb (BaFe<sub>12</sub>O<sub>19</sub>), as the samples were examined using an X-ray diffraction device, and it was found that the patterns of diffraction rays X-ray (XRD) for the three samples, respectively. I showed Results that All samples are polycrystalline, as shown tops X-ray diffraction of hexa- A with Miller coefficients (Miller indices) (103) and (110) and (107) and (114) and (206) when Bragg diffraction angles 2 θ are equal to 20.90 °, 30.39 °, 32.41 °, 34.30 °, and 42.58 °, respectively.

**Keywords-** Ferrite, hexagonal crystal structure, X-ray diffraction, structural properties.

## I. INTRODUCTION

The discovery of magnetic oxides has an important role in industrial and technological applications, as it contributed to the increase in the production of modern electronic devices closely related to these oxides [1-2], which are called conductive magnetic materials or ferrites, which are semi-conductive ferromagnetic materials and are characterized by a high density of materials. Important in technology and modern applications, these materials are characterized by their possession of high magnetic permeability, high electrical resistance up to (10<sup>9</sup> Ω) and a dielectric constant ranging between (10-5). Varied electronic with the passage of time [ 4-3]. In order to obtain a homogeneous compound, certain weight ratios of one or more supporting materials are added to the base material [5].

Hexaferrites are an important part of the magnetic oxides that have varying properties suitable for a wide range of technological and industrial applications [6-7]. For example, the magnetic properties of (M-type hexaferrite, A Fe<sub>12</sub> O<sub>19</sub>; A<sup>2+</sup> = Ba<sup>2+</sup>, Sr<sup>2+</sup>, Pb<sup>2+</sup>) can be modified to suit the requirements for different uses [9-8]. Since the discovery of ferrites in the 1950s, there has

been a great deal of interest in hexaferrites, also known as hexaferrites. [11-10]

## II. HEXAGONAL STRUCTURE HEXAGONAL

The hexagonal composition of ferrites was studied by the scientist Junker and his colleagues, where hexagonal ferrites were classified into six main types (U, W, M, X, Y, and Z). This classification depends on the chemical formula and crystal structure as listed in Table 1).

The crystal structure of the hexagons is described in several ways, including by S, R, and T, which represent segments or sites in the crystal structure called blocks, where S represents the spinal structure. and R [(Ba,Sr) Fe<sub>6</sub>O<sub>11</sub>], and T [(Ba,Sr) 2Fe<sub>8</sub>O<sub>14</sub>] Where the oxygen ions are a packed hexagonal crystal structure. This structure contains metal ions with radii close to oxygen. Hexagonal ferrites contain larger ions compared to garnet frites, and one of the most important hexagonal ferrites is the M type. It is the simplest species in terms of structure and general formula him) Fe<sub>12</sub>O<sub>19</sub> \_ \_ \_ (M where M is a divalent element usually the ions of the elements Ba, Sr or Pb Hexagonal ferrites are widely used

as permanent (solid) magnets and have high coercive strength that is used in higher frequency applications [12].

**Table 1: The type of hexagonal ferrites. [12]**

Type	Formula	Example
M-	MFe <sub>12</sub> O <sub>19</sub>	M= Ba, Pb, Sr
W-	MR <sub>2</sub> Fe <sub>16</sub> O <sub>27</sub>	R= Fe <sup>2+</sup> , Ni <sup>2+</sup> , Zn <sup>2+</sup> etc.
X-	MRFe <sub>28</sub> O <sub>46</sub>	
Y-	M <sub>2</sub> R <sub>2</sub> Fe <sub>12</sub> O <sub>22</sub>	
Z-	M <sub>3</sub> R <sub>2</sub> Fe <sub>12</sub> O <sub>41</sub>	
U-	M <sub>4</sub> R <sub>2</sub> Fe <sub>36</sub> O <sub>60</sub>	

### III. INITIAL MATERIALS PREPARATION

The raw materials shown in Table (1-3) were used in the preparation of the compounds under study PbFe<sub>12</sub>O<sub>19</sub> and BaFe<sub>12</sub>O<sub>19</sub> \_\_ and Pb (BaFe<sub>12</sub>O<sub>19</sub>).

**Table 2: The raw materials used.**

purity %	origin	Chemical formula	Subject Name
98%	HIMEDIA	PbO <sub>3</sub> _	Lead oxide
98%	INDIA	Fe <sub>2</sub> O <sub>3</sub> __	Iron oxide
98%	BDH	BaO	Barium oxide

### IV. STEPS OF SAMPLE PREPARATION

The manufacturing processes of some hexagonal polycrystalline compounds in general require several stages, which leads to an increase in the manufacturing cost, and these materials depend mainly and largely on the concentrations of their constituent elements and their purity. Therefore, the manufacturing process requires high accuracy at all stages in order to prevent pollution caused by impurities. The steps involved in the preparation were as follows:

#### 1- Preparing the materials:

The necessary raw materials have been prepared from the oxides mentioned in the previous table (1-3).

#### 2- Calculation of the weight ratios of the models:

The weight ratios of the materials included in the preparation of the models were accurately calculated using a sensitive balance of the German Sartorius type of high accuracy (within the range of 6-10 gram).

The weights of the compounds involved in the reaction are determined based on the molecular weight (M.Wt) of each element as follows:

Molecular weight of lead oxide (PbO<sub>2</sub>):  
M.Wt for PbO<sub>2</sub> = 207.2+2(15.999) = 239.19 gm /mole  
Partial weight of barium oxide (BaO):  
M.Wt for BaO = 137.3 + 15.999 = 153.3 gm /mole

And as an example for the preparation of mol 0.04 of one of the ferrite compounds prepared in this research, the weight ratios are calculated as follows:

M.Wt for BaO = 153.3 \* 0.04 = 6.13316 gm /mole  
M.Wt for PbO = 223.2 \* 0.04 = 9.5679 gm /mole  
M.Wt for Fe<sub>2</sub>O<sub>3</sub> = 159.69\*0.04 = 38.3256 gm /mole

#### 3- Mix Material:

A ceramic mortar was used to grind and mix the raw materials for 3 hr to obtain a homogeneous powder. The importance of this process lies in obtaining homogeneous powders that affect the physical properties of the final product.

#### 4- Heating:

The homogeneous mixture was heated to a temperature of 700 °C and for 4 hr, after placing it in a ceramic crucible, and then it is placed in an electric oven (MUFFLE FURNACE), where its temperature reaches 1200 °C. And Figure (2-3) shows a picture of the oven mentioned. This furnace is used for the purpose of primary conversion to ferroelectricity, which causes decomposition of the oxides that unite with each other to form structures different from the composition of the original oxides; As well as the evaporation of impurities, then left in the oven to gradually cool down to room temperature. And after it is taken out of the oven, it is ground again using the ceramic mortar and well for 1 hour. To obtain the best possible homogeneity of the mixture.



**Appearance 1: MUFFLE FURNACE electric oven, model SILMF-01**

#### 5- Adding the binder:

After the above grinding process, the binder is added, which is PVA (Poly Vinyl Alcohol). At a ratio of (2-3) drops for the purpose of cohesion of the mixture during its removal from the mold and the absence of surface defects in the model. This binder does not affect the main components of ferroelectric compounds because it evaporates during the heating process [13].

#### 6- Pressing:

A template with a diameter of 10 mm was manufactured for the purpose of performing the pressing process, and the prepared models were pressed using a mechanical hydraulic press under pressure (Ton). 4) over a period of time (min) (5) To obtain the sizes and shapes of the models that are appropriate to the requirements of the devices used for the purpose of conducting the required checks, and Figure (2) shows a picture of the manufactured template.



Figure 2: The factory mold.

#### 7- Annealing:

The finally compressed tablets are heated to a temperature (1000 °C) and for (4 hr). Using the electric oven mentioned in point 4 of this item, then the models are gradually cooled by leaving them inside the oven until they reach room temperature. And in this process, there is an internal diffusion of the adjacent particles, as they have the opportunity to be arranged, concentrated in their places, and cohesive with each other; The pores are reduced due to the spread of voids to the surface of the model. In the end, we get hard and less fragile ceramic models. It was observed that the diameter of the pattern decreases slightly after the annealing process, which works to reduce the pores due to the increase in the particle size [14]. Figure (3) below shows a picture of the models that have been prepared.

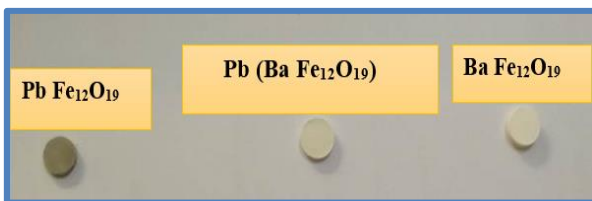


Figure 3: The models that were prepared after the annealing process.

#### 8- Coating with silver paste:

The two opposite surfaces of each model are coated with a thin layer of silver paste for the purpose of obtaining ohmic conductivity. ferroelectric models can be summarized According to the scheme shown in Figure (4) below.



Figure 4: The stages of manufacturing ferroelectric models using the method of solid state interactions.

## V. X-RAY DIFFRACTION TECHNIQUE

### 1- The Ultrastructural Assay's Structure Tests

To identify the crystal structures under study, the X-ray diffraction technique was relied upon using a Japanese device (SHIMADZU XRD 6000), whose image is shown in Figure (5), and with the specifications listed in Table (3) below:

**Table 3: Specifications of the X-ray diffraction machine.**

Target Type	Cuk $\alpha$
Wave Length	1.5418 Å
Scan Speed	8 deg /min
Current	30 Ma
Voltage	40 KV
Range 2 $\theta$	20o - 80o --

The X-ray diffraction pattern was diagnosed by recognizing the positions of the higher peaks that appear at Shine a beam of x-rays within range (80 ° - 20°) = 2 $\theta$  On the surface of the material, and as a result of the reflection of these rays from the surface of the parallel crystals, these reflected rays are intertwined with each other when the conditions that achieve Brack's law are met in the aforementioned equation [15].



**Figure 5: X-ray diffraction apparatus**

### 2- Density

The physical density of the models was measured through the ratio between the mass of each model when completely dry to its volume based on considering its homogeneous cylindrical shape through the following mathematical relationship [16]:

$$V = \pi r^2 h$$

r: represents the radius of the pattern ,h: thickness of the pattern, V: volume of the pattern.

Then the actual physical density is calculated  $\rho_a$  from the following mathematical relationship:

$$\rho_a = \frac{m}{V}$$

whereas:

$\rho_a$ : actual physical density.

m: mass of the model.

It is also possible to calculate some structural variables represented by lattice constants (a,c), particle size (D), forming factor and microcompliance for all models according to the equations mentioned in the previous chapter above. There are some variables that take a major role in changing the theoretical density, according to the production process and the nature of the materials used, including: the grinding and pressing process, as well as the chemical composition of the materials, in addition to that the size of the granules and their distribution plays an important role in changing the theoretical density.

X-ray diffraction models ( $\rho_{x-ray}$ ) through the following relationship [17]:

$$\rho_{x-ray} = \frac{n MW}{N_A V}$$

whereas:

n: the number of atoms per unit cell and its value is (1) for ferroelectric materials.

MWt: molecular weight

$N_A$ : Avogadro's number and its value is mol<sup>-1</sup> (6.023×10<sup>23</sup>).

V: the volume of the unit cell (a<sup>2</sup>c).

(P) in the prepared samples was also calculated; This is done using the following relationship [18]:

$$P = \left( \frac{\rho_{x-ray} - \rho_a}{\rho_{x-ray}} \right) \times 100\%$$

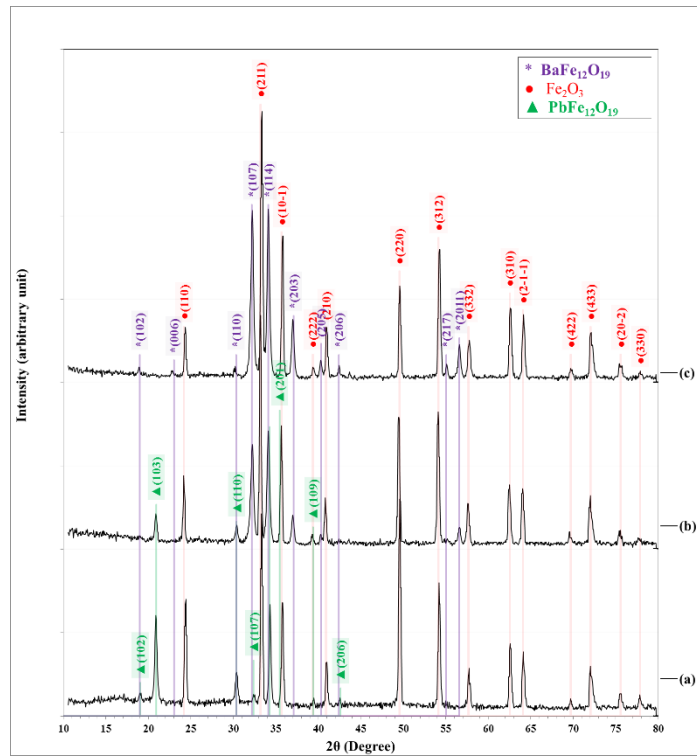
## VI. STRUCTURAL PROPERTIES

Figure shows 6 patterns diffraction rays X-ray (XRD) for the three samples, respectively. I showed Results that All samples are polycrystalline. The X-ray diffraction results also showed that sample A contains a mixture of two phases, Fe<sub>2</sub>O<sub>3</sub> and PbFe<sub>12</sub>O<sub>19</sub>, with a hexagonal structure according to for the two standard cards from The International Center for Diffraction Data (JCPDS) Same number (96-900-978 and 96-101-1083), respectively. as it appeared tops X-ray diffraction of hexa- A with Miller coefficients (Miller indices) (103) and (110) and (107) and (114) and (206) when Bragg diffraction angles  $\theta = 2, 20.90^\circ, 30.39^\circ, 32.41^\circ, 34.30^\circ$  and  $42.58^\circ$ , respectively. It is consistent with what the researcher stated [19].

You have a displacement minor in sites peaks because of stresses in the retina crystalline due to crystalline defects. As for sample C So he appeared They

consist of a mixture of two phases  $\text{Fe}_2\text{O}_3$  and  $\text{BaFe}_{12}\text{O}_{19}$  of hexagonal structure according to for the two standard JCPDS cards That paper m (96-900-978 and 96-900-8138). Where the hexagonal phase appeared with greater intensity than the sample that A. It is consistent with what the researcher stated [20]. It is worth noting that the

crystal structure of both hexagonal phases is  $\text{PbFe}_{12}\text{O}_{19}$  and  $\text{BaFe}_{12}\text{O}_{19}$  They are similar, but with a slight difference in their crystalline dimensions. While sample B showed a mixture of all phases  $\text{Fe}_2\text{O}_3$ ,  $\text{PbFe}_{12}\text{O}_{19}$  and  $\text{BaFe}_{12}\text{O}_{19}$  but in different proportions.



The Shape 6: Curves X-ray diffraction for samples (a)  $\text{PbFe}_{12}\text{O}_{19}$  and (b)  $\text{Pb}_{0.5}\text{Ba}_{0.5}\text{Fe}_{12}\text{O}_{19}$  and (c)  $\text{BaFe}_{12}\text{O}_{19}$ .

Distances between DHKL crystal planes were calculated From the Bragg equation depending on the x-ray diffraction angle  $\theta$  [21]

$$n \lambda = 2d_{hkl} \sin \theta$$

where  $\lambda$  represents the length waveform for rays Which is produced from a target of copper and equal to 0.154061 nm, while n diffraction order.

Well done account the size crystal using the offer full for lines X-ray diffraction (FWHM) using equation Debye- Scherer [22].

$$D = \frac{0.9 \lambda}{FWHM \cdot \cos(\theta)}$$

Table 1.4 shows the X-ray diffraction parameters of the X-ray diffraction lines for the three samples A, B, and C, as the table shows that the dominant phase in the three samples is  $\text{Fe}_2\text{O}_3$  with the presence of additional phases, which depend on the presence of added metals. The table shows the diffraction angles ( $2\theta$ ) and the widths of the peaks (FWHM). The relative intensity (I%) and the interlayer distances of the crystal planes ( $d_{hkl}$ ) and the crystal size (D) for each direction and the closest phase matched the location of the apex and Miller coefficients (hkl).

Schedule 4: Miller coefficients and interfacial distances for results XRD of the three models , respectively.

Sample	$2\theta$ (Deg.)	FWHM (Deg.)	I%	$d_{hkl}$ Std.(Å)	$d_{hkl}$ Exp.(Å)	D(nm)	hkl
A	20.9087	0.2913	47	4.2414	4.2452	27.7	(103)
	24.3884	0.3237	54	3.6775	3.6468	25.1	(110)
	30.3931	0.3075	20	2.9385	2.9386	26.8	(110)
	32.4162	0.3237	11	2.7622	2.7597	25.6	(107)
	33.2902	0.3075	94	2.6959	2.6892	27.0	(211)

	34.3098	0.2428	51	2.6171	2.6116	34.2	(114)
	35.7665	0.2751	53	2.5144	2.5085	30.3	(1-10)
	39.4243	0.2428	8	2.2884	2.2838	34.8	(222)
	40.9780	0.2751	27	2.2037	2.2007	30.8	(210)
	42.5803	0.2914	10	2.1207	2.1215	29.3	(206)
	49.6046	0.3399	100	1.8388	1.8363	25.7	(220)
	54.1850	0.2913	62	1.6924	1.6914	30.6	(312)
	57.7618	0.3561	22	1.5968	1.5949	25.5	(332)
	62.5526	0.3398	32	1.4842	1.4837	27.4	(310)
	64.1064	0.3561	30	1.4517	1.4515	26.3	(2-1-1)
	69.6902	0.3237	8	1.3479	1.3482	29.9	(422)
	72.0532	0.3723	23	1.3095	1.3097	26.4	(433)
	75.5491	0.4046	10	1.2572	1.2575	24.8	(20-2)
	77.8474	0.3561	9	1.2258	1.2260	28.7	(330)
B	20.9077	0.3075	15	4.2414	4.2454	26.3	(103)
	24.1457	0.2751	30	3.6775	3.6829	29.5	(110)
	30.4092	0.2913	10	2.9385	2.9371	28.3	(110)
	32.2058	0.3399	46	2.7791	2.7772	24.3	(107)
	33.1607	0.2590	100	2.6959	2.6994	32.0	(211)
	34.0994	0.3237	50	2.6268	2.6272	25.7	(114)
	35.6694	0.3399	53	2.5144	2.5151	24.6	(1-10)
	36.9965	0.3399	14	2.4232	2.4279	24.6	(203)
	39.2948	0.2752	7	2.2884	2.2910	30.7	(222)
	40.2659	0.2104	7	2.2037	2.2379	40.2	(210)
	40.8486	0.2751	22	2.2358	2.2074	30.8	(205)
	49.4751	0.2752	56	1.8388	1.8408	31.8	(220)
	54.1202	0.3399	59	1.6924	1.6932	26.2	(312)
	56.5965	0.3561	9	1.6254	1.6249	25.3	(2011)
	57.6162	0.3237	20	1.5968	1.5985	28.0	(332)
	62.4555	0.3561	28	1.4842	1.4858	26.1	(310)
	64.0254	0.3884	25	1.4517	1.4531	24.1	(2-1-1)
	69.5931	0.2913	8	1.3479	1.3498	33.2	(422)
	72.0532	0.4208	22	1.3095	1.3097	23.3	(433)
75.4844	0.3885	8	1.2572	1.2584	25.9	(20-2)	
77.7503	0.3722	5	1.2258	1.2273	27.4	(330)	
C	22.7538	0.3237	4	3.8657	3.9050	25.0	(006)
	24.3399	0.2590	20	3.6775	3.6540	31.4	(110)
	30.1988	0.2751	5	2.9465	2.9571	29.9	(110)
	32.1896	0.3399	62	2.7791	2.7786	24.3	(107)
	33.3387	0.3237	100	2.6959	2.6854	25.6	(211)
	34.0832	0.2914	63	2.6268	2.6284	28.5	(114)
	35.8150	0.2266	54	2.5144	2.5052	36.8	(1-10)
	37.0127	0.2913	23	2.4232	2.4268	28.8	(203)

39.4081	0.2428	6	2.2884	2.2847	34.8	(222)
40.2983	0.2751	8	2.2037	2.2362	30.8	(210)
40.9618	0.2428	20	2.2358	2.2015	34.9	(205)
42.4671	0.1942	6	2.1296	2.1269	43.9	(206)
49.6046	0.3075	35	1.8388	1.8363	28.5	(202)
54.2659	0.3075	49	1.6924	1.6890	29.0	(312)
55.0913	0.2590	7	1.6670	1.6657	34.6	(217)
56.6127	0.3237	14	1.6254	1.6245	27.9	(2011)
57.7780	0.3399	16	1.5968	1.5944	26.7	(332)
62.5526	0.3075	27	1.4842	1.4837	30.2	(310)
64.1387	0.3237	25	1.4517	1.4508	29.0	(2-1-1)
69.7711	0.4208	5	1.3479	1.3468	23.0	(422)
72.1179	0.3722	18	1.3095	1.3087	26.4	(433)
75.5815	0.3884	6	1.2572	1.2571	25.9	(20-2)
77.8960	0.3722	4	1.2258	1.2254	27.4	(330)

In the samples were calculated based on the ratio of the sum of the intensity of the diffraction peaks that belong to the phases that were distinguished in the previous table using the relationship:

$$\% \text{ of Chemical composite phase} = \frac{\sum J_A}{\sum J_A + \sum J_B + \sum J_C}$$

As shown in Table 5. It appears from the table that the ratio of the crystalline phase PbFe<sub>12</sub>O<sub>19</sub> in sample A is 22%, while the maximum percentage was 78% for the Fe<sub>2</sub>O<sub>3</sub> phase. It also appeared that the ratio of crystalline phases in sample B it is 4.3% for phase PbFe<sub>12</sub>O<sub>19</sub> and 23.7% for the phase BaFe<sub>12</sub>O<sub>19</sub> and 72.1% for the Fe<sub>2</sub>O<sub>3</sub> phase. While the phase ratios for the C sample were 36% for the phase BaFe<sub>12</sub>O<sub>19</sub> and 64.0% for the Fe<sub>2</sub>O<sub>3</sub> phase. The increase in the hexagonal phase ratio with barium compared with lead is due to the different oxidation susceptibility of the three metals.

**Schedule 5: The crystalline ratios of the chemical compounds in the three samples in a row after the thermal process.**

Sample	PbFe <sub>12</sub> O <sub>19</sub> %	BaFe <sub>12</sub> O <sub>19</sub> %	Fe <sub>2</sub> O <sub>3</sub> %
A	22.0	0.0	78.0
B	4.3	23.7	72.1
C	0.0	36.0	64.0

It was completed to choose The two peaks (103 and ) 110 (for the crystal structure of PbFe<sub>12</sub>O<sub>19</sub> and the two peaks (107) and ) 114 (for the crystal structure of BaFe<sub>12</sub>O<sub>19</sub> From X-ray diffraction to account Parameters network ) a And c (for the hexagon using a computational program based on the relation of the hexagonal structure: [ 23 ]

$$\frac{1}{d_{hkl}^2} = \frac{4}{3} \frac{h^2 + hk + k^2}{a^2} + \frac{l^2}{c^2}$$

where *d* represents *hkl* she distances between levels crystalline and (hkl) transactions Miller .while the volume was calculated cell Unit V) using Relationship For the hexagonal structure [24]:

$$V = a^2 \cdot c \sin(120^\circ) = a^2 \cdot c \frac{\sqrt{3}}{2}$$

The unit cell density of the composite reticule was calculated using the relation [24]:

$$\rho = \frac{z \cdot M \cdot W_t}{V \cdot N_A}$$

*z* represents the number of molecules per unit cell = 2, MW is the molecular weight of the compound and is calculated from the sum of the atomic weights of the elements, *N<sub>A</sub>* Avogadro's number and *V* is the volume of the unit cell.

Table 6 shows lattice constants (*a* and *c*), unit cell size and density in terms of X-ray diffraction for samples A and B and C, respectively, as it is evident that the crystalline dimensions and crystalline size increased For samples that contain barium compared to samples containing lead, the average crystal size also increased, as the addition of this element acted as a catalyst for crystal growth, so we notice a decrease in density for samples that contain barium for two reasons. Less atomic weight than lead. It is worth mentioning here that this slight change in the dimensions of the lattice has a significant impact on the physical properties of the compound such as optical, electrical and mechanical properties due to the difference in the bond energy between the atoms [ 24].

**Table 6: Average crystal size and lattice constants (a,c) for the hexagonal phase and unit cell size for samples A And B And C on respectively .**

Sample	Ave. D(nm)	PbFe <sub>12</sub> O <sub>19</sub> _ _ _			BaFe <sub>12</sub> O <sub>19</sub> _ _ _		
		a (Å)	c (Å)	V(Å <sup>3</sup> )	a (Å)	c (Å)	V(Å <sup>3</sup> )
A	28.09	5.8772	23.0852	690,568	-	-	-
B	28.02	5.8742	23.1161	690,778	5.8959	23.1673	697,431
C	29.77	-	-	-	5.8985	23.1790	698,413

Table 7 shows the physical density of the three samples calculated from the sample dimensions (diameter and thickness) and its mass compared to the density indicative of the X-ray diffraction of the samples A And B And C on respectively. From these two values of density, the ratio of the gaps inside the samples and the porosities (Porosity) was calculated based on the equation [25] :

$$\text{Porosity} = (1 - \rho / \rho_x) * 100$$

It is clear that the porosity increased from 3.39 to 38.28% for the samples when replacing lead with barium.

**Table 7: Average crystal size, lattice constants for the hexagonal phase, unit cell size and density calculated for the three samples.**

Sample	Mass (g)	Diameter (cm)	Thickness (cm)	$\rho$ (g/ cm <sup>3</sup> )	$\rho_x$ (g/cm <sup>3</sup> )	Porosity (%)
A	1.1780	0.91	0.33	5.4886	5.6813	3.39
B	0.9200	0.91	0.33	4.2865	5.4852	21.85
C	0.7001	0.91	0.33	3.2619	5.2852	38.28

## VII. RESULTS

- 1- That All samples are polycrystalline, as shown tops X-ray diffraction of hexa- A with Miller coefficients (Miller indices) (103) and (110) and (107) and (114) and (206) when Bragg diffraction angles  $2\theta$  are equal to 20.90 °, 30.39 °, 32.41 °, 34.30 °, and 42.58 °, respectively.
- 2- Find a displacement minor in sites peaks because of stresses in the retina crystalline due to crystalline defects. As for sample C So he appeared They consist of a mixture of two phases Fe<sub>2</sub>O<sub>3</sub> and BaFe<sub>12</sub>O<sub>19</sub> of hexagonal structure according to For the two standard JCPDS cards That paper m (96-900-978 and 96-900-8138).
- 3- The crystal structure of both hexagonal phases is PbFe<sub>12</sub>O<sub>19</sub> and BaFe<sub>12</sub>O<sub>19</sub> They are similar, but with a slight difference in their crystalline dimensions
- 4- Sample B showed a mixture of all phases Fe<sub>2</sub>O<sub>3</sub>, PbFe<sub>12</sub>O<sub>19</sub> and BaFe<sub>12</sub>O<sub>19</sub> but in different proportions.

## REFERENCES

[1] Smit , J. and Wijn , HPJ, "Ferrites", ( Wiley, New York, 1959).  
 [2] Mahmood, SH, "Permanent Magnet Applications", in: SH Mahmood  
 [3] PS Aghav , VN Dhage , ML Mane , DR Shengule , RG Dorik , and KM Jadhav , "Effect of aluminum substitution on the structural and magnetic properties of cobalt ferrite synthesized by solgel auto combustion

process", Physica B: Condensed Matter, 406(23), 4350 (2011).  
 [4] M. Sugimoto, "Past, Present, and Future of Ferrites", Journal of American Ceramuc Society, 82, 1 (1999).  
 [5] Nikhilesh Chawla & Krishan K. Chawla , "Metal Matrix Composites", Journal of Material Science, 2(3), 1 (1986).  
 [6] Harris, VG, Geiler , A., Chen, Y., Yoon, SD, Wu, M., Yang, A., Chen, Z., He, P., Parimi , P.V. and Zuo , X., Journal of Magnetism and Magnetic Materials, 321 (2009) 2035.  
 [7] Kamishima , K., Hosaka , N., Kakizaki , K. and Hiratsuka, N., Journal of Applied Physics, 109 (2011) 013904.  
 [8] Mahmood, SH and Bsoul , I., "Tuning the magnetic properties of M-type hexaferrites ", in: RB Jotania and SH Mahmood (Eds.) Magnetic Oxides and Composites, (Materials Research Forum LLC, Millersville, PA, USA, 2018), p. 49-100.  
 [9] Topal , U., Journal of Superconductivity and Novel Magnetism, 25 (2012) 1485.  
 [10] Sabah Muhammad Ali, "Study and Design of Microwave Absorption Ferrite Materials in the X-Beam Range." PhD thesis, University of Technology 2000 .  
 [11] S. Sindhu, "Preparation and Characterization of Spinel Ferrites - Their Incorporation in Rubber Matrix And Evaluation of Properties," no. April. p. 141, 2001.  
 [12] KJ Standley , *Oxide magnetic materials* : 2nd ed., Clarendon Press, Oxford, 1972.

- [13] Salman, Muhammad :A study of the physical properties of  $Ni_{1-x}Cd_xFe_2O_4$  compounds prepared by the powder technology method , Master Thesis ,University of Tikrit, (College of Education) ,(2015) .(
- [14] Jassim, Najwa Abdel-Jabbar: “A study of the structural and electrical properties of  $Pb(Zr, Ti)O_3$  compounds prepared by the powder technique”, Master Thesis, University of Tikrit, (College of Education) ) , (2015 )
- [15] Kumar, S. and Chandra, R.” Temperature dependent studies of CdS nano -particles in viscous matrix” , *Optical Materials*, 27, (2005), 1346-1349.
- [16] Paul, T. C. \_Simon Jacques Advanced Certificate in Powder Diffraction on the Web. Bragg's Law (2006).
- [17] Rani, R .; Kumar, P.; Juneja , JK; Raina , KK and Prakash , C. “Dielectric properties of  $0.95(Pb_{1-3x/2}La_xZr_{0.65}Ti_{0.35}O_3)-0.05(Ni_{0.8}Zn_{0.2}Fe_2O_3)$  composites”, *Advances in Condensed Matter Physics*, 637170 , (2011), 1-5.
- [18] Naiden , EP, VI Itin , and OG Terekhova . “ Mechanochemical modification of the phase diagrams of hexagonal oxide ferrimagnets .” *Technical Physics Letters* 29.11 (2003): 889-891.
- [19] HJL Hillary, S. Xavier, and P. Praveen, “St. Joseph 's Journal of Structural, Vibrational, Morphological and Magnetic Properties of Copper Ferrite Nano Particles (  $Cu_{0.4}Mg_{0.6}Fe_2O_4$  ) by Co-precipitation, *St. Joseph's J. Humanit. Sci.* , no. November, p. 2–7, 2019.
- [20] M. Maddahfar, M. Ramezani, and S. Mostafa Hosseinpour-Mashkani, “Barium hexaferrite/graphene oxide: controlled synthesis and characterization and investigation of its magnetic properties,” *Appl. Phys. A mater. Sci. Process.* , vol. 122, no. 8, p. 1–9, 2016.
- [21] WH Bragg and WL Bragg, *X Rays and Crystal Structure* . London: G. Bell and Sons, LTD., 1918.
- [22] SK Pendyala, K. Thyagarajan, A. Gurusampath Kumar, and L. Obulapathi, “Investigations on physical properties of Mg ferrite nanoparticles for microwave applications,” *J. Microw. Power Electromagne. Energy* , vol. 53, no. 1, p. 3–11, 2019.
- [23] L. Glasser and HDB Jenkins, “Lattice Energies and Unit Cell Volumes of Complex Ionic Solids,” *J. Am. Chem. Soc.* , vol. 122, no. 4, p. 632–638, 2000.
- [24] N. Malde, PSIPN de Silva, AKM Akther Hossain, LF Cohen, KA Thomas, JL MacManus-Driscoll, ND Mathur, and MG Blamire, “Influence of oxygen stoichiometry on Raman phonon spectroscopy, lattice parameters and physical properties of  $La_{0.7}Ca_{0.3}MnO_3$  thin films,” *Solid State Commun.* , vol. 105, no. 10, p. 643–648, 1998.
- [25] H. Chen, Z. Zhao, H. Xiang, F.-Z. Dai, J. Zhang, S. Wang, J. Liu, and Y. Zhou, “Effect of reaction routes on the porosity and permeability of porous high entropy  $(Y_{0.2}Yb_{0.2}Sm_{0.2}Nd_{0.2}Eu_{0.2})B_6$  for transpiration cooling ,” *J. Mater. Sci. Technol.* , vol. 38, p. 80–85,